nature research

https://doi.org/10.1038/s41586-020-03159-7

Supplementary information

Correlation-driven topological phases in magic-angle twisted bilayer graphene

In the format provided by the authors and unedited

Supplementary Information: Correlation-driven Topological Phases in Magic-Angle Twisted Bilayer Graphene

Youngjoon Choi, Hyunjin Kim, Yang Peng, Alex Thomson, Cyprian Lewandowski, Robert Polski, Yiran Zhang, Harpreet Singh Arora, Kenji Watanabe, Takashi Taniguchi, Jason Alicea, Stevan Nadj-Perge

Theoretical Modeling

Hofstadter spectrum from Continuum model We will follow the approach used in Ref. 1,2. The continuum model Hamiltonian for TBG at K-valley (in monolayer graphene BZ) can be written in the following matrix form

$$H = \begin{pmatrix} h_-(-\theta/2) & T(\boldsymbol{r}) \\ T(\boldsymbol{r})^\dagger & h_+(+\theta/2) \end{pmatrix} \tag{1}$$

where the intralayer Hamiltonian is given by

$$h_\mp(\mp\theta/2) = \hbar v_F(\hat{\boldsymbol{p}} + \boldsymbol{q}_h) \cdot \boldsymbol{\sigma}_{\mp\theta/2}, \tag{2}$$

and the interlayer coupling is written as $T(\boldsymbol{r}) = w\sum_{j=0}^{2} T_j \exp(-i\boldsymbol{q}_j \cdot \boldsymbol{r})$. Here, $\boldsymbol{q}_0 = k_\theta(0,-1)$, $\boldsymbol{q}_1 = k_\theta(-\sqrt{3},1)/2$, $\boldsymbol{q}_2 = k_\theta(\sqrt{3},1)/2$, $\boldsymbol{q}_h = k_\theta(\sqrt{3}/2,0)$, $k_\theta = 8\pi\sin(\theta/2)/(3a)$. The matrices are defined as $T_0 = \eta\sigma_0 + \sigma_1$, $T_1 = \eta\sigma_0 + \zeta\sigma_+ + \bar{\zeta}\sigma_-$, $T_2 = \eta\sigma_0 + \zeta\sigma_- + \bar{\zeta}\sigma_+$, with $\zeta = \exp(i2\pi/3)$, where the Pauli matrices $\sigma_{1,2,3}$, $\sigma_\pm = (\sigma_1 \pm i\sigma_2)/2$ correspond to the sublattice degree of freedom. In the following, we choose the Fermi velocity $v_F = 9.38 \times 10^6$ m/s, the interlayer coupling strength $w = 110$ meV, and $\eta = 0.4$ which takes into account the effects of lattice relaxation.

In the presence of perpendicular magnetic field $\boldsymbol{B} = B\hat{\boldsymbol{z}}$, we substitute $\hat{\boldsymbol{p}} \to \hat{\boldsymbol{p}} + e\boldsymbol{A}$. We further take the Landau gauge $\boldsymbol{A} = B(-y, 0)$.

We can rewrite the intralayer Hamiltonian as

$$h_\mp(\mp\theta/2) = \hbar\omega_c \begin{pmatrix} 0 & a_{p_x} e^{\pm i\theta/2} \\ a_{p_x}^\dagger e^{\mp i\theta/2} & 0 \end{pmatrix} \tag{3}$$

where $\omega_c = \sqrt{2}v_F/l_b$, $l_b = \sqrt{\hbar/eB}$, and

$$a_{p_x} = \frac{1}{\sqrt{2}}\left[((\hat{p}_x + \frac{\sqrt{3}}{2}k_\theta)l_b - y/l_b) - i\hat{p}_y l_b\right] \tag{4}$$

$$a_{p_x}^\dagger = \frac{1}{\sqrt{2}}\left[((\hat{p}_x + \frac{\sqrt{3}}{2}k_\theta)l_b - y/l_b) + i\hat{p}_y l_b\right] \tag{5}$$

Numerically, we can diagonalize the Hamiltonian using the basis $\{|L,\sigma,n;k\rangle = |k\rangle \otimes |L,\sigma,n,k\rangle\}$ (truncated up to some index n), where $L = \mp$ is the layer index, σ is the sublattice index, and $\hat{p}_x|k\rangle = k|k\rangle$, and n labels the nth harmonic oscillator eigenstates such that $a_k|n,k\rangle = \sqrt{n}|n-1,k\rangle$, $a_k^\dagger|n,k\rangle = \sqrt{n+1}|n+1,k\rangle$. Moreover, we have

$$a_k = \exp(-i\tilde{p}_y k l_b^2) a \exp(i\tilde{p}_y k l_b^2), \tag{6}$$

with $a \equiv a_0$, and $\exp(-i\hat{p}_y k l_b^2)|n,0\rangle = |n,k\rangle$.

Let us compute the matrix elements of the Hamiltonian in the above basis.

Intralayer Hamiltonian. In this basis, the annihilation operator has the following matrix elements

$$\langle L',\sigma',n';k'|a_k|L,\sigma,n;k\rangle = \sqrt{n-1}\delta_{kk'}\delta_{LL'}\delta_{\sigma\sigma'}\delta_{n',n-1} \tag{7}$$

Interlayer Hamiltonian. The matrix elements of the interlayer Hamiltonian can be evaluated using

$$\langle -,\sigma',n';k'|T_j e^{-i\boldsymbol{q}_j\cdot\boldsymbol{r}}|+,\sigma,n;k\rangle = (T_j)_{\sigma'\sigma}\delta_{k',k-q_{jx}} e^{-iq_{jy}kl_b^2} e^{-iq_{jy}\sqrt{3}k_\theta l_b^2/2} e^{iq_{jx}q_{jy}l_b^2/2} F_{n',n}(z_j) \tag{8}$$

where $z_j = \frac{q_{jx}+iq_{jy}}{\sqrt{2}} l_b$.

The function $F_{n',n}(z)$ is

$$F_{n',n}(z) = \begin{cases} \sqrt{\frac{n!}{n'!}}(-\bar{z})^{n'-n}\exp(-|z|^2/2)L_n^{(n'-n)}(|z|^2) & n' \geq n \\ \sqrt{\frac{n'!}{n!}} z^{n-n'}\exp(-|z|^2/2)L_{n'}^{(n-n')}(|z|^2) & n' < n. \end{cases} \tag{9}$$

Hofstadter spectrum from the ten-band model Here, we briefly describe the ten-band model for the TBG at magic angle, first introduced in Ref. 3.

The ten-band model is defined on a triangular lattice with basis vectors $\boldsymbol{a}_1 = (\sqrt{3}/2, -1/2)$ and $\boldsymbol{a}_2 = (0,1)$. We write the Bravais lattice sites as $\boldsymbol{r} = r_1\boldsymbol{a}_1 + r_2\boldsymbol{a}_2$ or simply as $\boldsymbol{r} = (r_1, r_2)$, where $r_{1,2} \in \mathbb{Z}$. Within each unit cell, there are ten orbitals which are distributed on three different sites, as indicated by the different colors in Fig. 1. Explicitly, there are three orbitals, p_z, p_+, and p_-, on every triangular lattice site (orange).

Each of the three kagome sites (black) within a unit cell hosts an s orbital. Finally, both A and B sublattices of the honeycomb sites (green) have p_+ and p_- orbitals. Throughout this work, these ten orbitals are ordered as $c_{\boldsymbol{r}} = \left(\tau_{z,\boldsymbol{r}}, \tau_{+,\boldsymbol{r}}, \tau_{-,\boldsymbol{r}}, \kappa_{1,\boldsymbol{r}}, \kappa_{2,\boldsymbol{r}}, \kappa_{2,\boldsymbol{r}}, \eta_{A+,\boldsymbol{r}}, \eta_{A-,\boldsymbol{r}}, \eta_{B+,\boldsymbol{r}}, \eta_{B-,\boldsymbol{r}}\right)^T$, where τ, κ, and η denote operators on the triangular, kagome, and honeycomb sites respectively.

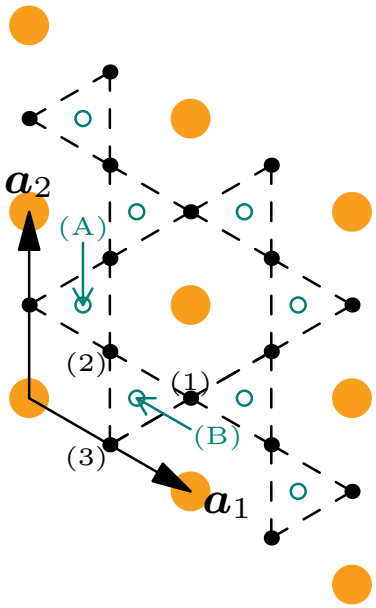

Supplementary Information Figure 1 | Lattice and orbitals for the ten-band model. The orange solid circles denote the triangular sites with p_z, p_+, and p_- orbitals. The black solid circles correspond to the three types of kagome sites, labeled as (1), (2), and (3). On each of these kagome sites, there is an s orbital. The green empty circles indicate the honeycomb sites, either type A or type B, with p_+ and p_- orbitals on each of them.

When an external perpendicular magnetic field is applied, we insert a Peierls phase $\exp(i\theta_i j)$ with

$$\theta_i j = \frac{e}{\hbar}\int_{\boldsymbol{r}_i}^{\boldsymbol{r}_j} \boldsymbol{A}\cdot d\boldsymbol{l} \tag{10}$$

into the hopping amplitude from $\boldsymbol{r}_i$ to $\boldsymbol{r}_j$.

When the flux per unit cell is a rational number p/q, with $p, q \in \mathbb{Z}$, namely

$$\Phi = \frac{p}{q}\phi_0, \quad \phi_0 = \frac{hc}{e}, \tag{11}$$

we can take the periodic Landau gauge[4]

$$\boldsymbol{A} = \frac{p\phi_0}{2\pi q}\left[(\xi_1 - \lfloor\xi_1\rfloor)\boldsymbol{b}_2 - \xi_2\sum_{n=-\infty}^{\infty}\delta(\xi_1 - n + 0^+)\boldsymbol{b}_1\right], \tag{12}$$

where $\boldsymbol{b}_1$ and $\boldsymbol{b}_2$ are reciprocal lattice vectors. The advantage of the periodic Landau gauge is the system is periodic in both $\boldsymbol{a}_1$ and $\boldsymbol{a}_2$ directions, with periods $\boldsymbol{a}_1$ and $q\boldsymbol{a}_2$, respectively.

References:

1. Bistritzer, R. & MacDonald, A. H. Moiré butterflies in twisted bilayer graphene. *Phys. Rev. B* **84**, 035440 (2011). URL https://link.aps.org/doi/10.1103/PhysRevB.84.035440.

2. Hejazi, K., Liu, C. & Balents, L. Landau levels in twisted bilayer graphene and semiclassical orbits. *Phys. Rev. B* **100**, 035115 (2019). URL https://link.aps.org/doi/10.1103/PhysRevB.100.035115.

3. Po, H. C., Zou, L., Senthil, T. & Vishwanath, A. Faithful tight-binding models and fragile topology of magic-angle bilayer graphene. *Phys. Rev. B* **99**, 195455 (2019). URL https://link.aps.org/doi/10.1103/PhysRevB.99.195455.

4. Hasegawa, Y. & Kohmoto, M. Periodic landau gauge and quantum hall effect in twisted bilayer graphene. *Phys. Rev. B* **88**, 125426 (2013). URL https://link.aps.org/doi/10.1103/PhysRevB.88.125426.